

Suppression of Excitation and Spectral Broadening Induced by Interactions in a Cold Gas of Rydberg Atoms

Kilian Singer,^{*} Markus Reetz-Lamour, Thomas Amthor, Luis Gustavo Marcassa,[†] and Matthias Weidemüller[‡]
Physikalisches Institut der Universität Freiburg, Hermann-Herder-Str.3, 79104 Freiburg, Germany[§]

(Dated: October 9, 2018)

We report on the observation of ultralong range interactions in a gas of cold Rubidium Rydberg atoms. The van-der-Waals interaction between a pair of Rydberg atoms separated as far as 100,000 Bohr radii features two important effects: Spectral broadening of the resonance lines and suppression of excitation with increasing density. The density dependence of these effects is investigated in detail for the S- and P- Rydberg states with main quantum numbers $n \sim 60$ and $n \sim 80$ excited by narrow-band continuous-wave laser light. The density-dependent suppression of excitation can be interpreted as the onset of an interaction-induced local blockade.

PACS numbers: 32.80.Rm, 32.80.Pj, 34.20.Cf, 03.67.Lx

With the advances in laser cooling and trapping, new perspectives for the investigation of Rydberg atoms [1] have been opening. When cooled to very low temperatures, the core motion can be neglected for the timescales of excitation (“frozen Rydberg gas”). Unexpected effects have been discovered, such as the many-body diffusion of excitation [2, 3], the population of high-angular-momentum states through free charges [4], or the spontaneous formation and recombination of ultracold plasmas [5, 6]. Other fascinating features of cold, interacting Rydberg atoms have been proposed but not been observed so far, e.g. the creation of ultralong range molecules [7, 8], whereas molecular crossover resonances have already been found experimentally [9]. One outstanding property of Rydberg atoms is their high polarizability, caused by the large distance between the outer electron and the core. This leads to strong electric field sensitivity and strong long-range dipole-dipole and van-der-Waals (vdW) interactions are expected. First indications of interaction effects between Rydberg gases at high densities have been found in an atomic beam experiment [10] and, more recently, collisional evidence for ultralong range interactions in a cold Rydberg gas has been reported [11]. In a frozen gas these interactions make Rydberg atoms possible candidates for quantum information processing [12, 13]. One promising approach is based on the concept of a dipole blockade [13], *i.e.* the inhibition of multiple Rydberg excitations in a confined volume due to interaction-induced energy shifts.

In this Letter we report on experimental evidence for ultralong range interactions in a frozen Rydberg gas and we present high-resolution spectroscopic signatures of these interactions. Similar indications of suppressed excitation have recently been observed in pulsed Rydberg ex-

citation from a cold gas [14]. Different to these findings, our experiment makes use of a tunable narrow-bandwidth continuous-wave (cw) laser for Rydberg excitation and thus allows for high-resolution spectroscopy of the resonance lines. By varying the density of Rydberg atoms in a controlled way, the influence of interactions on the strength and the shape of these lines is investigated in detail. Signatures of ultralong range interactions appear as spectral broadening of the excitation lines and saturation of the resonance peak height, the latter being an indication of the dipole blockade.

To realize a frozen gas of Rydberg atoms we trap ⁸⁷Rb atoms in a dispenser-loaded magneto-optical trap (MOT). The MOT is located inside a vacuum chamber (background pressure 5×10^{-11} mbar) which provides optical access along three main orthogonal axes and two diagonals. The MOT coils are located inside the vacuum chamber. The trapping laser light is provided by a diode laser system consisting of two diode lasers which are simultaneously injection-locked to a frequency-stabilized extended cavity diode laser (ECDL) at 780 nm and added coherently [15]. The output of this laser-addition setup is sent through a single-mode optical fiber for mode cleaning providing about 70 mW at the output. The frequency is detuned by 1.5Γ (natural line width $\Gamma/2\pi = 6.1$ MHz) to the red of the cooling and trapping transition $5S_{1/2}(F=2) \rightarrow 5P_{3/2}(F=3)$. A second ECDL drives the repumping transition $5S_{1/2}(F=1) \rightarrow 5P_{3/2}(F=2)$. The MOT contains $1.2(3) \times 10^7$ atoms at temperatures around 100 μ K. The atom cloud can be approximated by a Gaussian spatial distribution with an $1/e$ diameter of 1.2(0.3) mm resulting in peak densities of $1.1(3) \times 10^{10}$ cm⁻³, as determined by absorption imaging with a resonant probe laser beam [16].

The laser light for driving the transition to Rydberg states $5P_{3/2}(F=3) \rightarrow n\ell_j$ is provided by a commercial laser system (Toptica, TA-SHG 110) consisting of an ECDL at 960 nm subsequently amplified to 1W and then frequency doubled to 479 nm with a line width < 2 MHz. The output beam which can be switched by an acousto-optical modulator (AOM) is guided along one of the diagonal axes of the vacuum chamber and focused to a waist

^{*}Electronic address: kilian.singer@physik.uni-freiburg.de

[†]Instituto de Física de São Paulo, Caixa Postal 369, 13560-970, São Carlos, São Paulo, Brazil

[‡]Electronic address: m.weidemueller@physik.uni-freiburg.de

[§]URL: <http://quantendynamik.physik.uni-freiburg.de>

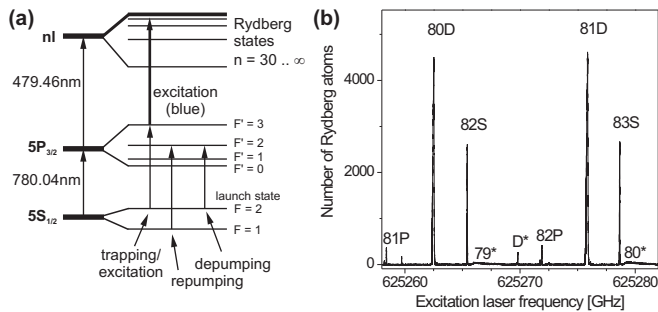


FIG. 1: (a) Relevant energy levels of ^{87}Rb addressed by transitions driven by the trapping laser, the repumping and the depumping lasers at 780 nm, and the Rydberg excitation laser at 479 nm. (b) Rydberg spectrum at main quantum number $n \sim 80$. The small D* line is attributed to a hyperfine ghost excited from the $5S_{1/2}(F=1)$ state. The small structures labeled 79* and 80* are hydrogen-like states with $\ell \geq 3$.

of $80(10)\mu\text{m}$ at the center of the atom cloud. The overlap between the atom cloud and the blue laser beam defines an effective Rydberg excitation volume $V_{\text{exc}} = 1.1 \text{ mm}^3$.

The two-step excitation into Rydberg states is schematically shown in Fig. 1(a). At the beginning of an excitation cycle, the trapping laser is tuned into resonance with the $5S_{1/2}(F=2) \rightarrow 5P_{3/2}(F'=3)$ transition. Subsequently, the blue Rydberg excitation laser which is tuned to the Rydberg manifold is switched on for typically $20\mu\text{s}$. Rydberg atoms are accumulated in the excitation volume during this time, since the lifetime of the Rydberg states exceeds $100\mu\text{s}$ [1, 17]. After the Rydberg excitation laser is blocked, the trapping laser is reset to the MOT detuning of -1.5Γ . The Rydberg atoms are field-ionized by applying a voltage of 40 Volts to the central field plates consisting of nickel meshes separated by 13.2 mm with 95% transparency through which the MOT beams pass almost unperturbed. The ions are accelerated onto a micro-channel plate detector (MCP). Residual electrical fields during Rydberg excitation are mainly caused by the MCP potential of -1.9kV . Field components perpendicular to the field plates are compensated by applying a small voltage, while parallel field components are measured to be less than 0.16 V/cm . The excitation cycle is repeated every 20 ms while maintaining a continuously loaded steady-state MOT. To take an excitation spectrum, the frequency of the blue laser is scanned at a rate of 300 MHz/s .

The density of Rydberg atoms can be controlled by varying the population in the $5S_{1/2}(F=2)$ launch state through optical pumping into the $5S_{1/2}(F=1)$ state. For this purpose, the repumping laser is attenuated by an AOM while an additional depumping laser resonant with the transition $5S_{1/2}(F=2) \rightarrow 5P_{3/2}(F=2)$ (see Fig. 1(a)) is switched on. Within 1 ms, the density of atoms in the launch state is lowered by one order of magnitude, as is measured by recording the fluorescence on the closed $5S_{1/2}(F=2) - 5P_{3/2}(F=3)$ transition with a photodiode. Note that no atoms are lost from the MOT capture

volume during this short period of time, and that the excitation volume V_{exc} remains unaltered. By delaying the two-step Rydberg excitation scheme with respect to the start of the depumping process, one can thus modify the density of atoms in the launch state without changing the total density of atoms in the MOT.

Absolute numbers of Rydberg atoms per excitation cycle are obtained by comparing the number of atoms lost from the trap, as deduced from the change in fluorescence rate at 780 nm, with the integral of the ion signal at the MCP. In this way, the response of the MCP can be calibrated and nonlinearities at large ion signals are compensated. Throughout this paper, the number of Rydberg atoms is derived from the number of measured ions at the MCP after calibration. Peak Rydberg densities \hat{n}_{Ryd} are calculated by dividing the number of Rydberg atoms by the effective excitation volume V_{exc} , assuming that the spatial distribution of Rydberg atoms follows the distribution of ground state atoms. We estimate the systematic error for the absolute number and peak density of Rydberg atoms to be a factor of roughly 3.

A Rydberg spectrum for $n \sim 80$ is depicted in Fig. 1(b). About 4500 Rydberg atoms are detected for the strong dipole-allowed D transitions. The resonance line width is typically $\sim 30 \text{ MHz}$ caused by saturation broadening of the first excitation step [18]. Dipole-forbidden P states are also excited due to the residual electrical field. Under our experimental conditions, the ion formation rate for $n \sim 80$ states through blackbody radiation [1] is estimated from calculated lifetimes [17] to be approximately 200Hz. Ionization rates due to collisions of cold Rydberg atoms with residual hot Rydberg atoms are of the same order of magnitude assuming an upper limit of 10^8 cm^{-3} for the densities of hot Rydberg atoms. We therefore do not expect significant effects of spontaneous creation of ions and avalanche processes during the timescales of excitation ($\sim 20 \mu\text{s}$) [5].

To study interaction effects between Rydberg atoms, excitation spectra of the $82S_{1/2}$ state are recorded for different Rydberg densities. The density is changed by either varying the power of the excitation laser or, as described above, by changing the density \hat{n}_g of atoms in the $5S_{1/2}(F=2)$ launch state. Figs. 2(a1) and 2(a2) are taken at low intensity of the blue excitation laser ($I = 6 \text{ W/cm}^2$). In this “low power regime”, the line shows no broadening. The number, and thus the density, of Rydberg atoms increases with \hat{n}_g , as the number of launch state atoms in the fixed excitation volume increases. The behavior changes drastically at higher intensity of the blue excitation laser. Figs. 2(a3) and (a4) show the resonance line at an excitation intensity of about 500 W/cm^2 . In the “high power” regime characterized by Rydberg densities in the 10^8 cm^{-3} range, one observes an asymmetric broadening of the line. Qualitatively similar line broadenings at Rydberg densities around 10^{11} cm^{-3} were observed earlier in an atomic beam experiment [10]. The line broadenings are attributed to level shifts of Ryd-

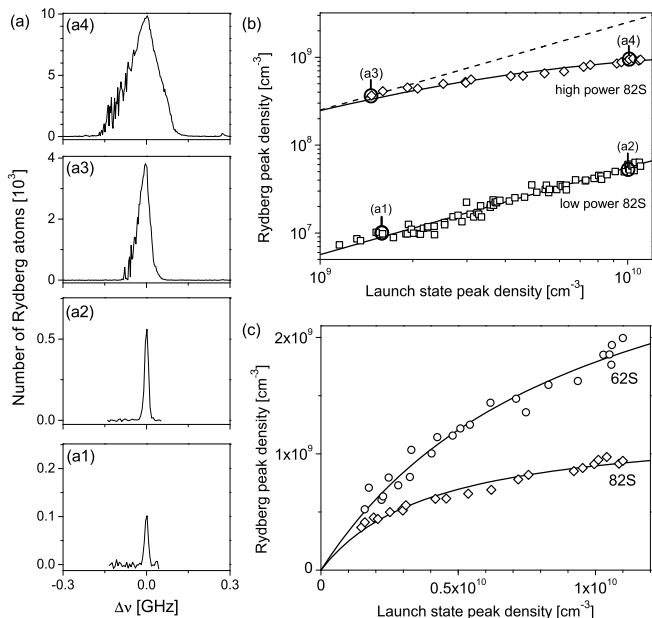


FIG. 2: (a) Excitation spectra of the $82S_{1/2}$ state at different intensities of the blue excitation laser [6 W/cm^2 for (a1) and (a2), 500 W/cm^2 for (a3) and (a4)] and launch state densities [(a1) $1.6 \times 10^9 \text{ cm}^{-3}$, (a2) $1.0 \times 10^{10} \text{ cm}^{-3}$, (a3) $1.5 \times 10^9 \text{ cm}^{-3}$, (a4) $1.0 \times 10^{10} \text{ cm}^{-3}$]. (b) Rydberg peak densities on the $82S_{1/2}$ resonance versus launch state density for 6 W/cm^2 (\square) and 500 W/cm^2 (\diamond). The dashed line is a linear extrapolation from the origin through the first data point. Data points corresponding to the spectra (a1) to (a4) are marked. (c) Comparison of the density-dependent suppression of Rydberg excitation for the $82S_{1/2}$ (same data as in (b)) and $62S_{1/2}$ (\circ) resonances. The $62S_{1/2}$ data was taken at 350 W/cm^2 . The solid lines in (b) and (c) show fitted saturation functions (see text).

berg states induced by the long-range vdW interactions of Rydberg atom pairs, although an appropriate model describing these line shapes is still lacking. Our high-resolution spectra in a cold gas reveal additional spectral features in the red wing of the resonance line, which show strong shot-to-shot fluctuations. Since these features never appear at the blue side of the resonance, independent of the scanning direction, one is tempted to attribute them to molecular resonances in the attractive part of an interaction potential. The origin of the fluctuating resonances remains to be clarified.

The line broadening is accompanied by suppression of excitation on resonance. In Fig. 2(b) we have plotted the peak density of Rydberg atoms excited on resonance versus peak density \hat{n}_g of $5S_{1/2}$ ($F = 2$) atoms for both the “low power” and the “high power” regimes. If no interaction was present, the peak density of Rydberg atoms scales linearly with \hat{n}_g . This is indeed realized in the “low power” regime as a fit to the data yields $\hat{n}_{\text{Ryd}} = p_{82,\text{low}} \hat{n}_g^{0.99(2)}$ with a probability $p_{82,\text{low}} = 0.006(1)$ for an atom to become excited in a Rydberg state during the

$20\text{-}\mu\text{s}$ excitation interval. In the “high power” regime, however, the increase of Rydberg density scales less than linear with \hat{n}_g clearly showing a suppression of excitation. At high excitation rate and density, we detect only 10^4 Rydberg atoms, which is a factor of ~ 2.7 less than expected from simple linear density scaling (see dashed line in Fig. 2(b)). The data is fitted by a heuristic saturation function of the form $\hat{n}_{\text{Ryd}} = p_{82,\text{high}} \hat{n}_g / (1 + \frac{\hat{n}_g}{n_{\text{sat}}})$ giving $p_{82,\text{high}} = 0.31(2)$ and $n_{\text{sat}} = 4.1(4) \times 10^9 \text{ cm}^{-3}$. The deviation of $p_{82,\text{high}}/p_{82,\text{low}} = 56$ from the ratio of the blue excitation laser power of 83 indicates a slight power saturation of the Rydberg excitation. It is important to note that power saturation can neither explain the asymmetric broadening of the excitation lines nor can it explain the *density-dependent* saturation of the Rydberg excitation. Saturation caused by the MCP detection is excluded by the calibration and linearization procedure. Therefore we attribute the suppression of the Rydberg excitation to interatomic interactions resulting in the onset of a dipole blockade caused by vdW interactions.

To further test this interpretation we have compared the saturation for different main quantum numbers n . The vdW interaction potential between two Rydberg atoms strongly increases with n . Therefore, one expects weaker suppression of Rydberg excitation for lines with lower main quantum number, although the transition strength of these lines is much higher as it scales with $(n^*)^{-3}$ where n^* denotes the main quantum number corrected by the corresponding quantum defect [1]. Fig. 2(c) shows a comparison of resonantly excited Rydberg atoms on the $82S_{1/2}$ line and the $62S_{1/2}$ line. The solid lines show fits of the saturation function described above. For the $62S_{1/2}$ line we find $p_{62,\text{high}} = 0.37(2)$ and $n_{\text{sat}} = 9(1) \times 10^9 \text{ cm}^{-3}$. The $62S_{1/2}$ saturation density is larger by more than a factor of 2 than the saturation density of the $82S_{1/2}$ excitation. Additionally, the asymptotic Rydberg density ($p_{\text{Ryd}} n_{\text{sat}}$ for $\hat{n}_g \gg n_{\text{sat}}$) for $62S_{1/2}$ relative to $82S_{1/2}$ is larger by factor of 2.8. Both findings support the interpretation in terms of an interaction-induced blockade.

We have also studied the density dependence of the dipole-forbidden fine structure doublet $81P_{1/2}$ and $81P_{3/2}$ (left and right peak in Fig. 3(a), respectively), for which theoretical calculations of the pair potentials are available [19, 20]. Two features are remarkable: With increasing density the $81P_{3/2}$ peak develops a wing on the red side of the resonance, again with the fluctuating resonances (see also Fig. 2(a)), while the $81P_{1/2}$ peak is hardly broadened, but grows much faster with the launch state density. As shown in Fig. 3(b), the attractive $81P_{3/2}$ interaction asymptote is much steeper than the $81P_{1/2}$ asymptote due to a coincidental near-resonant enhancement in the C_6 coefficient. This explains why broadening is only observed for the red wing of the $81P_{3/2}$ line but not for the $81P_{1/2}$ line. The average nearest neighbor distances derived from the launch state density are depicted by the dashed lines in Fig. 3(b). The red broadening starts when the average nearest neighbor

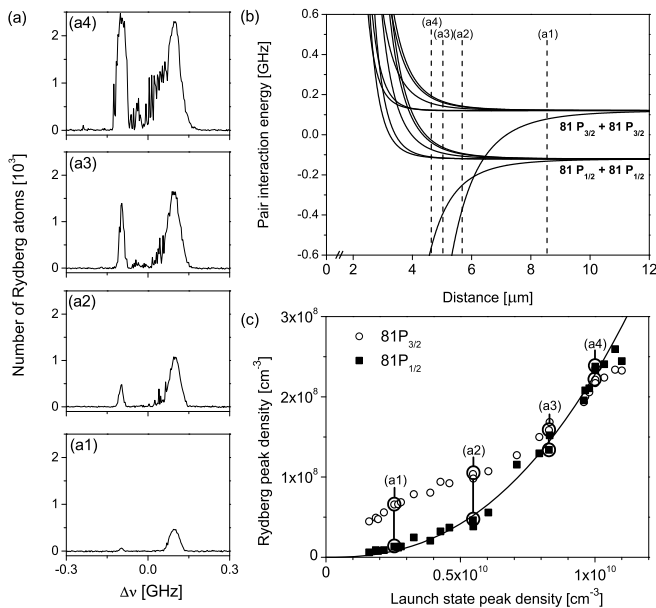


FIG. 3: (a) Resonance line for the fine structure doublet $81P_{1/2}$ (left) and $81P_{3/2}$ (right) at excitation intensity of about 500 W/cm^2 and different launch state densities [(a1) $2.5 \times 10^9 \text{ cm}^{-3}$, (a2) $5.5 \times 10^{10} \text{ cm}^{-3}$, (a3) $8.3 \times 10^9 \text{ cm}^{-3}$, (a4) $1.0 \times 10^{10} \text{ cm}^{-3}$]. (b) Calculated vdW pair potentials for the $81P_{1/2} + 81P_{1/2}$ and $81P_{3/2} + 81P_{3/2}$ asymptote versus the interatomic distance. Dashed lines indicate the average nearest neighbor distances $\hat{n}_g^{-1/3}$ for the corresponding spectra in (a). (c) Resonance peak densities of the $81P_{1/2}$ and the $81P_{3/2}$ line as a function of the launch state peak density. The solid line is a polynomial fit to the data. The data points corresponding to the graphs depicted in (a) are marked.

distance becomes comparable to interatomic distances at which the attractive interaction potential starts to bend, and observed broadening and interaction energy are within the same order of magnitude.

Contrary to the dipole-allowed S and D lines, the dipole-forbidden $81P_{1/2}$ and $81P_{3/2}$ peaks grow much faster than linear with the launch state density \hat{n}_g , as shown in Fig. 3(c). A fit to the data of the $81P_{1/2}$ resonance yields a scaling with $\hat{n}_g^{2.4(1)}$. The behavior of the $81P_{3/2}$ peak is more complicated, but shows saturation relative to the $81P_{1/2}$ peak, which may again be caused

by a interaction-induced blockade effect. Whether the density dependence of the dipole-forbidden P lines may be attributed to interaction-induced S- and D-admixtures in addition to the admixture caused by the residual static electric field ($< 0.16 \text{ V/cm}$) has to be clarified in the framework of a detailed model for the cw Rydberg excitation in a cold gas.

In conclusion, we have explored two signatures of interactions in a cold Rydberg gas by controlling the density: A broadening of Rydberg resonance lines with additional spectral features in the red wings and a suppression of on-resonance excitation. We find qualitative agreement between the observed broadening with predicted pair-interaction vdW potentials in the case of the $81P$ fine-structure doublet. Theoretical calculations of vdW potentials including fine structure are needed to allow for a more quantitative description of the observed line shapes.

The saturation of Rydberg excitation with increasing launch state density is a complementary signature of the ultralong range Rydberg-Rydberg interactions and marks the onset of a vdW-induced dipole blockade. While the spectral broadening of the resonance lines can only be understood as an “instantaneous” excitation of Rydberg pairs, it is not clear whether the density-dependent saturation occurs in a similar way or whether it is induced by a process based on the successive creation of Rydberg atoms. The latter hypothesis has successfully been employed in the interpretation of similar saturation effects recently observed for Rydberg atoms excited through short duration, high intensity laser pulses from a cold gas [14]. Our experimental approach employing narrow-band cw Rydberg excitation can directly be applied to the implementation of quantum information processing with Rydberg atoms [13, 21] by further increasing the density, thus proceeding from the two-body limit to the full many-body regime of the dipole blockade.

The project is supported in part by the Landesstiftung Baden-Württemberg in the framework of the “Quantum Information Processing” program and by the DAAD-PROBRAL program. We acknowledge contributions from S. Fölling and M. Tschernack. We are also indebted to D. Schwalm for generous support at the Max-Planck-Institute for Nuclear Physics. We thank R. Côté, P. Gould and E. Eyler for valuable discussions and providing us with the $81P$ potentials.

-
- [1] T. F. Gallagher, *Rydberg Atoms* (Cambridge University Press, Cambridge, 1994).
 - [2] I. Mourachko et al., Phys. Rev. Lett. **80**, 253 (1998).
 - [3] R. C. Stoneman et al., Phys. Rev. Lett. **58**, 1324 (1987).
 - [4] S. Dutta et al., Phys. Rev. Lett. **86**, 3993 (2001).
 - [5] M. Robinson et al., Phys. Rev. Lett. **85**, 4466 (2000).
 - [6] T. F. Gallagher et al., J. Opt. Soc. Am. B **20**, 1091 (2003).
 - [7] C. H. Greene et al., Phys. Rev. Lett. **85**, 2458 (2000).
 - [8] C. Boisseau et al., Phys. Rev. Lett. **88**, 133004 (2002).
 - [9] S. Farooqi et al., Phys. Rev. Lett. **91**, 183002 (2003).
 - [10] J. Raimond et al., J. Phys. B **14**, L655 (1981).
 - [11] A. L. de Oliveira et al., Phys. Rev. Lett. **90**, 143002 (2003).
 - [12] D. Jaksch et al., Phys. Rev. Lett. **85**, 2208 (2000).
 - [13] M. D. Lukin et al., Phys. Rev. Lett. **87**, 037901 (2001).
 - [14] D. Tong et al., arXiv:physics/0402113 (2004).
 - [15] K. Singer et al., Opt. Comm. **218**, 371 (2003).
 - [16] We estimate a factor of 2 as the systematic error for the determination of the density and number of atoms.

- [17] C. E. Theodosiou (2000), priv. comm.
- [18] Broadening by the Zeeman shift in the inhomogeneous MOT magnetic field is below 5 MHz.
- [19] R. Côté, priv. comm.
- [20] M. Marinescu, Phys. Rev. A **56**, 4764 (1997).
- [21] B. K. Teo et al., Phys. Rev. A **68**, 053407 (2003).